Zn Incorporation in Hydroxy-Al- and Keggin Al13-Intercalated Montmorillonite: A Powder and Polarized EXAFS Study

ARTICLE *in* ENVIRONMENTAL SCIENCE AND TECHNOLOGY · APRIL 2007

Impact Factor: 5.33 · DOI: 10.1021/es061958i · Source: PubMed

Environ. Sci. Technol. **2007**, *41,* 1942−1948

Zn Incorporation in Hydroxy-Al- and Keggin Al_{13}-Intercalated Montmorillonite: A Powder and Polarized EXAFS Study

MICHEL L. SCHLEGEL*,† AND ALAIN MANCEAU‡

CEA - Laboratory for the Reactivity of Surfaces and Interfaces and UMR 8587, DEN/DPC/SCP/LRSI, CEA of Saclay, F-91191 Gif-sur Yvette Cedex, France, and Environmental Geochemistry Group, Maison des Géosciences, Université J. Fourier and CNRS, BP 53, F-38041 Grenoble Cedex 9, France

The sorption mechanism of Zn on gibbsite and montmorillonite exchanged with Al^{3+} (Al-mont) or Keggin Al_{13} polymer (Al_{13}-mont) was probed by powder and polarized EXAFS spectroscopy as a function of pH (5.85−7), reaction time (1−65 days), and sorbate to sorbent ratio (50−200 μM Zn/2 g montmorillonite). For all Al-mont samples, Zn is octahedrally coordinated to oxygens at ∼2.08(2) Å, and surrounded in-plane by six Al atoms at 3.02−3.06(2) Å, and another six at 6 Å. No out-of plane Si neighbors are detected. These results are interpreted as Zn incorporation in vacant octahedral sites of gibbsite-like layers at the basal and/or interlayer surface of montmorillonite particles. Zinc sorbed on the edges of gibbsite layers would give a split first oxygen shell with bond distances of 2.00(2) and 2.16(3) Å, and 2.1(8) nearest Al at 3.02 Å with no second-nearest Al, none of which were observed in Al-mont. The binding environment of Zn on Al_{13}-mont after 1 day is similar to that on the edges of gibbsite, and is interpreted as Zn complexation at the surface of Al polymers. After 28 days, the Zn environment resembles that of Zn-sorbed Al-mont, indicating the progressive buildup of Zn-containing gibbsite-like layers parallel to montmorillonite layers. The results of this work clarify the incorporation mechanism of Zn in hydroxy-Al interlayered phyllosilicate and provide insight on the formation mechanism of this common Zn species in soil.

Introduction

The design of nuclear waste repositories and in situ remediation of contaminated sites face similar problems of limiting the transport and bioavailability of radionuclides and metals. In both cases, cost-effective confinement and in situ sequestration strategies entail the use of inorganic sorbents for the retention of (radio)toxic elements. Clay minerals are choice materials due to their high sorption capacities (*1*). Experimental work has shown that the affinity of trace metals for montmorillonite is increased by cationic exchange with Al (Al-mont) and Keggin Al_{13} polymer (Al_{13}-mont) (*2*−*6*). However, the binding mechanism of metals on Al-modified smectites cannot be clarified at the molecular-level by wet chemical approaches only.

Important progress in clay reactivity research has been accomplished by using polarized extended X-ray absorption fine structure (P-EXAFS) spectroscopy (*7*). The nature of reactive surface sites and sorption mechanism of trace elements on clays often can be determined unambiguously by this technique (*8*−*15*). For example, P-EXAFS was used to elucidate the structural mechanism of Zn uptake on montmorillonite at pH 7.3 and its dependence on the concentration of dissolved silicon ($[Si]_{aq}$). Zinc forms mononuclear inner-sphere complex at the edges of montmorillonite layers at low $[Si]_{aq}$ (∼70 μM), and precipitates epitaxially as kerolite at $[Si]_{aq}$ relevant to geochemical systems (∼500 μM) (*14*). In contrast, Zn is in a gibbsite-like (α-$Al(OH)_3$) environment in Al-mont at acidic pH (*16*), but the nature of sorption sites, the structural relationship of the gibbsitic layers with the clay particles, and the formation mechanism of this Zn species are unknown. This information is important because this last species is widespread (*16*−*18*). Here, relevant data were obtained by applying P-EXAFS to Zn sorbed on Al-mont and Al_{13}-mont as a function of pH, sorbate/sorbent ratio, and reaction time.

Materials and Methods

A detailed description of the materials and experimental methods is given in the Supporting Information (SI). Briefly, the <2 μm fraction of MX-80 montmorillonite was isolated and purified using standard techniques (*14*). The structural formula of the purified montmorillonite is $Na_{0.28}(Al_{1.61}Mg_{0.24}Fe^{3+}_{0.13}Fe^{2+}_{0.02})(Si_{3.98}Al_{0.02})O_{10}(OH)_2$, the cation exchange capacity calculated from clay composition is 760 meq kg^{-1}, and the specific surface area estimated from morphology is 788 m^2 g^{-1} (*19*, *20*). Mass indications refer to the purified suspension, regardless of clay exchange with Al or Al_{13}. Al-mont was prepared by titrating Al-exchanged montmorillonite to pH 5 (*5*). An Al_{13} solution was obtained by slow stepwise titration of 0.25 M $AlCl_3$ with 1 M NaOH at 80 °C (*4*). Al_{13}-mont was obtained by montmorillonite washings in the Al_{13} solution. Aliquots of the Al-mont and Al_{13}-mont suspensions were transferred and dried on a glass slide for characterization by X-ray diffraction at room pressure of water vapor (Phillips X'Pert diffractometer).

Zn Uptake Experiments. Uptake experiments were conducted at 25.0 ± 0.1 °C (thereafter, the condensed notation 25.0(1) °C is used for uncertainties), under a nitrogen atmosphere. A high Na concentration of 0.5 M was maintained using NaCl (Sigma-Aldrich). The pH values were measured with a combination electrode (Metrohm). Suspension pHs were adjusted to, and maintained at, the desired pH for the first week of the experiments by computer-controlled addition of acid or base solutions. Chemical conditions were $[Zn]_{tot}$ = 50 μM, pH = 6 (AlMt-50-6), $[Zn]_{tot}$ = 50 μM, pH = 7 (AlMt-50-7), $[Zn]_{tot}$ = 200 μM, pH = 7 (AlMt-200-7) for Al-mont; and $[Zn]_{tot}$ = 100 μM, pH = 6 (Al_{13}Mt-100-6) for Al_{13}-mont (Table 1). The solutions were sampled, centrifuged, and filtered (Whatman 0.1 μm cellulose nitrate) periodically to determine solute Zn, Si, and Al concentrations in the filtered supernatant ($[Zn]_{aq}$, $[Si]_{aq}$, and $[Al]_{aq}$). Self-standing films of Zn-sorbed Al-mont or Al_{13}-mont were prepared by filtering 30 mL of suspension on 0.01 μm Millipore cellulose nitrate filters. Highly textured self-supporting films are obtained by this technique (*7*, *8*, *10*).

EXAFS Data Collection and Reduction. Zn K-edge EXAFS spectra were recorded at the European Synchrotron Radiation

* Corresponding author phone: +33 1 69 08 93 84; fax: +33 1 69 08 54 11; e-mail: Michel.Schlegel@cea.fr.

† CEA - Laboratory for the Reactivity of Surfaces and Interfaces and UMR 8587.

‡ Université J. Fourier and CNRS.

10.1021/es061958i CCC: $37.00
Published on Web 02/17/2007

TABLE 1. Samples Analyzed by EXAFS Spectroscopy

sample name	sorbent	[sorbent][a] (g L^{-1})	pH	$[Zn]_{tot}$[b] (μM)	Zn uptake[c] (%)	time[d] (d)
AlMt-200-7-1d	Al-mont	2.0	7.0	200	99.3	1
AlMt-200-7-35d	Al-mont	2.0	7.0	200	99.6	35
AlMt-50-7-1d	Al-mont	2.0	7.0	50	99.3	1
AlMt-50-7-6d	Al-mont	2.0	7.0	50	99.1	6
AlMt-50-7-64d	Al-mont	2.0	7.0	50	99.0	64
AlMt-50-6-1d	Al-mont	2.0	6.0	50	98.9	1
AlMt-50-6-42d	Al-mont	2.0	6.0	50	99.0	42
Zn-sorbed-HIM[e]	Al-mont	15	5.0	15,000		15
Zn-coprec-HIM[e]	Al-mont	15	4.5	15,000		15
Al_{13}Mt-100-6-1d	Al_{13}-mont	2.0	6.0	100	39	1
Al_{13}Mt-100-6-28d	Al_{13}-mont	2.0	5.85	100	33.5	28
Zn-sorbed-gibbsite[f]	gibbsite	5	6.0	1000	14.9	1

[a] Concentration of sorbent in suspension. [b] Amount of Zn added to the suspension. [c] Amount of Zn sorbed on the sorbent. [d] Reaction time in days. [e] Zn sorbed on, or coprecipitated in, hydroxy-Al sheets intercalated between montmorillonite layers. From ref *16*. [f] Spectrum J from ref *28*.

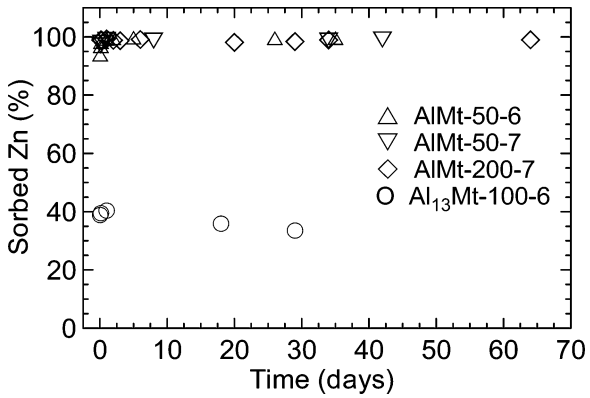

FIGURE 1. (a) Zinc uptake as a function of time, pH, $[Zn]_{tot}$, and nature of sorbent. The concentration of Al-mont and Al_{13}-mont in all experiments was 2 g L^{-1}. (△): pH 6, $[Zn]_{tot}$ = 50 μM. (▽): pH 7, $[Zn]_{tot}$ = 50 μM. (◇): pH 7, $[Zn]_{tot}$ = 200 μM. (○): pH 6, $[Zn]_{tot}$ = 100 μM.

Facility (ESRF, France) on the FAME beamline (*21*). All spectra were recorded in fluorescence-yield detection mode, using a 30 element array Ge detector. EXAFS spectra ($\chi(k)$) were extracted from raw data using standard procedures (*22*). Fourier transformations were performed on $k^3\chi(k)$ functions using a Kaiser apodization window (*23*). The FT peaks of interest were selected and fitted in the *R*-space. The goodness of the fits was quantified by the R_p parameter (*14*).

Results and Interpretations

X-ray Diffraction. The X-ray diffractogram for Al-mont had a well-defined 001 reflection with a d_{001} spacing (uncorrected for structure factor) of 15.2 Å. This value is somewhat lower than those reported previously (15.9 Å; (*5*), and 16.1 Å; (*3*)), suggesting that the clay was incompletely exchanged. Also, Al was probably irregularly inserted between clay layers because higher-order 00*l* reflections were absent. The Al_{13}-mont diffractogram had a 001 reflection at 19.5 Å, a slightly higher value than reported in the literature (18.8 Å) (*5*, *24*). Higher order 00*l* reflections were present, indicating a uniform insertion of Al_{13} polymers in successive interlayers.

Zinc Uptake. Nearly complete Zn uptake occurred within the first hour of reaction in Al-mont suspensions (Figure 1) as Zn has a high affinity for this sorbent (*5*, *6*). Zinc uptake by Al_{13}Mt-100-6 was limited to ~39% of $[Zn]_{tot}$ (19 μmol g^{-1}) in the first day of experiment, in agreement with previous studies (*5*). Zn uptake decreased to 33% of $[Zn]_{tot}$ (17 μmol g^{-1}) after 28 days, likely as a result of the decrease of the suspension pH from 6 to 5.85. For Al-mont experiments, $[Si]_{aq}$ plateaued after ~20 days at 55−56, 35, and 22 μM for AlMt-50-6, AlMt-200-7, and AlMt-50-7, respectively (Figure S1a in Supporting Information). In the Al_{13}-mont experiment, $[Si]_{aq}$ increased steadily from 3 to 42 μM over 28 days. The dissolution rate for this last experiment (1.1×10^{-11} mol s^{-1} g^{-1}) is about 1 order of magnitude greater than that reported by Furrer et al. at pH 5 (1.4×10^{-12} mol s^{-1} g^{-1}) (*4*), a difference, however, well within the variability in dissolution rates for montmorillonite (*25*). The $[Al]_{aq}$ values in Al-mont suspensions hovered around 3−6 μM (Figure S1b), i.e., about 1 order of magnitude higher than the solubility limit of gibbsite (~0.3 μM) (*26*). In Al_{13}Mt-100-6, $[Al]_{aq}$ was as high as 480 μM at the uptake onset and increased to 754 μM after 28 days (Figure S1c). The high $[Al]_{aq}$ values likely result from the buildup of Al polymers in suspension (*5*). These polymers may be Al_{13} aggregates or Al hydroxides formed from the decomposition of Al_{13} polymers (*27*).

EXAFS Spectroscopy. *EXAFS Spectra.* All powder spectra are structured and have multiple wave frequencies from well-ordered atomic shells around Zn (Figure 2a). Aside from Al_{13}-Mt-100-6-1d and Zn-sorbed gibbsite (*28*), they all look similar, with a strong absorption dip near 3.9 $Å^{-1}$. This feature was reported previously for Zn sorbed on Al-mont (Zn-sorbed-HIM) and coprecipitated with Al in montmorillonite (Zn-coprec-HIM; Table 1) (*16*), and is characteristic of the exclusive presence of Al atoms in the first cationic shell of Zn (*18*, *29*). The spectra of Al_{13}Mt-100-6-1d and Zn-sorbed-gibbsite have strong similarities, and thus Zn has a similar binding environment in the two samples. In Zn-sorbed gibbsite, Zn is tetrahedral (^{IV}Zn) and octahedral (^{VI}Zn), and Zn polyhedra are bonded through edge-sharing to Al octahedra (*28*). Spectra for AlMt-200-7-1d, AlMt-200-7-35d, and Al_{13}Mt-100-6-28d have a strong angular dependence (Figure 3a), meaning that the Zn coordination shells are oriented with respect to clay platelets. The Zn shells are much less oriented in Al_{13}Mt-100-6-1d, but still significantly anisotropic.

Fourier Transforms and Quantitative Analysis. Except for Al_{13}Mt-100-6-1d and Zn-sorbed-gibbsite, all powder FTs have intense peaks at $R + \Delta R$ ~1.6 Å (peak A), ~2.6 Å (peak B), and ~5.5 Å (peak C) (Figure 2b). Peak C is weak in Al_{13}Mt-100-6-1d and absent in Zn-sorbed gibbsite.

Peak A is produced by the Zn−O atomic pair in the first shell (O_1). The position of the imaginary part (Im(FT)) and magnitude (|FT|) maximum of the FT depend on the Zn−O_1 distance, which in turn depends on the number of oxygen atoms coordinated to Zn (*30*). For example, peak A is shifted to smaller $R + \Delta R$ distance in Zn-sorbed gibbsite relative to Zn-sorbed HIM because Zn is 4-fold (^{IV}Zn) and 6-fold (^{VI}Zn) coordinated in the first reference, and only octahedral in the second (Figure 2b) (*16*, *28*). The O_1 shell of Zn-sorbed gibbsite was best-fitted with 4.1(6) O_{1A} at $R^{EXAFS}_{Zn-O_{1A}}$ = 2.00(2) Å and

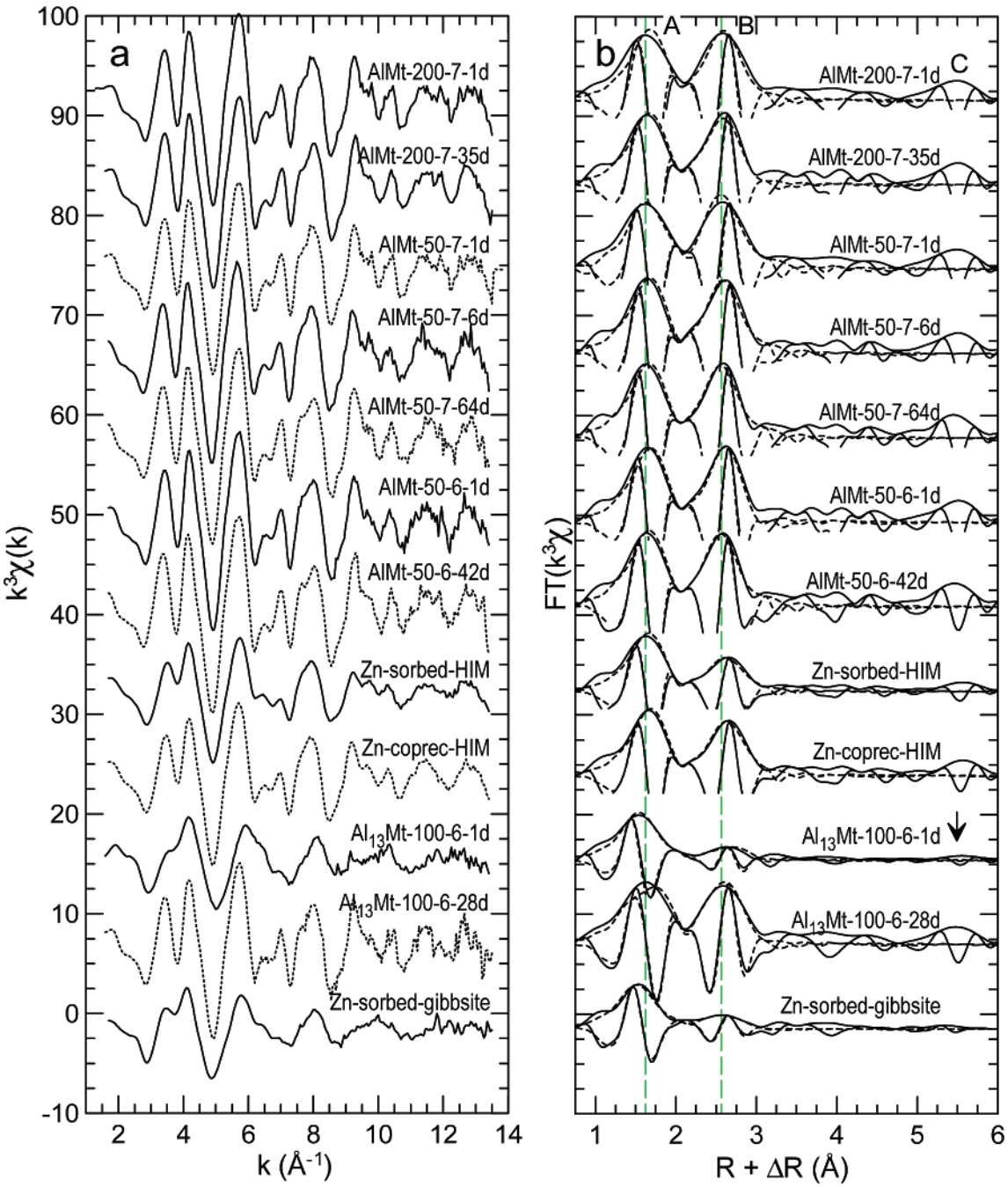

FIGURE 2. (a) k^3-weighted Zn K-edge powder EXAFS spectra for Zn-sorbed Al-mont and Al_{13}-mont. All spectra were recorded on self-supporting films and at the magic angle ($\alpha = 35°$). Also plotted are the spectra for Zn-sorbed HIM and Zn-coprecipitated HIM from ref *16*, and Zn-sorbed gibbsite from ref *28*. (b) Moduli and imaginary parts of the Fourier transforms (FT) for the data (solid line) and spectral simulations (dashed lines).

1.9(6) O_{1B} at $R^{EXAFS}_{Zn-O_{1B}} = 2.16(4)$ Å ($\sigma = 0.081$ Å) (Table S1 in Supporting Information). The two distances average out to 2.00(2) Å, in agreement with the mean distance of 2.01 Å reported previously for the same spectrum (*28*). The O_1 shell of Al_{13}Mt-100-6-1d, the peak A of which is at the same position as that of Zn-sorbed-gibbsite, was best-fitted with 3.4(4) O_{1A} at $R^{EXAFS}_{Zn-O_{1A}} = 1.97(2)$ Å and 2.2(2) O_{1B} at $R^{EXAFS}_{Zn-O_{1B}}$ 2.12(2) Å ($\sigma = 0.067$ Å). In the two samples, the O_{1A} subshell is attributed to ^{IV}Zn, and the O_{1B} subshell is attributed to ^{VI}Zn (*14*, *28*). The assumption of a unique O_1 shell at $R^{EXAFS}_{Zn-O_{1B}} = 2.07-2.09$ Å ($\sigma = 0.08-0.09$ Å) yielded optimal fits to all other data, indicating that Zn is exclusively octahedral in Al-mont and in Al_{13}-mont after 28 days of reaction time (Table S1).

Peak B in Zn-sorbed-HIM and Zn-coprec-HIM has been attributed to Al atoms at ~3.05−3.06 Å (*16*). Here, this assignment is confirmed by the near coincidence in position of the maxima of |FT| and Im(FT). Otherwise, when Zn is surrounded predominantly by high-z cations, as in Zn-rich phyllosilicate and Zn−Al layer double hydroxide, |FT| is a maximum when Im(FT) is a minimum (Figure S2 in Supporting Information). Thus we can conclude from Figure 2b that Al atoms predominate in the second shell around Zn for all sorption samples. The rounded shape of the first EXAFS oscillation for Zn-sorbed gibbsite and Al_{13}Mt-100-6-1d is due to the fewer number of Zn−Al pairs, as their peak B has low amplitude.

The amplitude of peak B is maximum at $\alpha = 10°$ and continuously decreases with increasing α (Figure 3b). If Zn was coordinated to cations in the in-plane and out-of-plane directions, then the angular dependence of peak B would

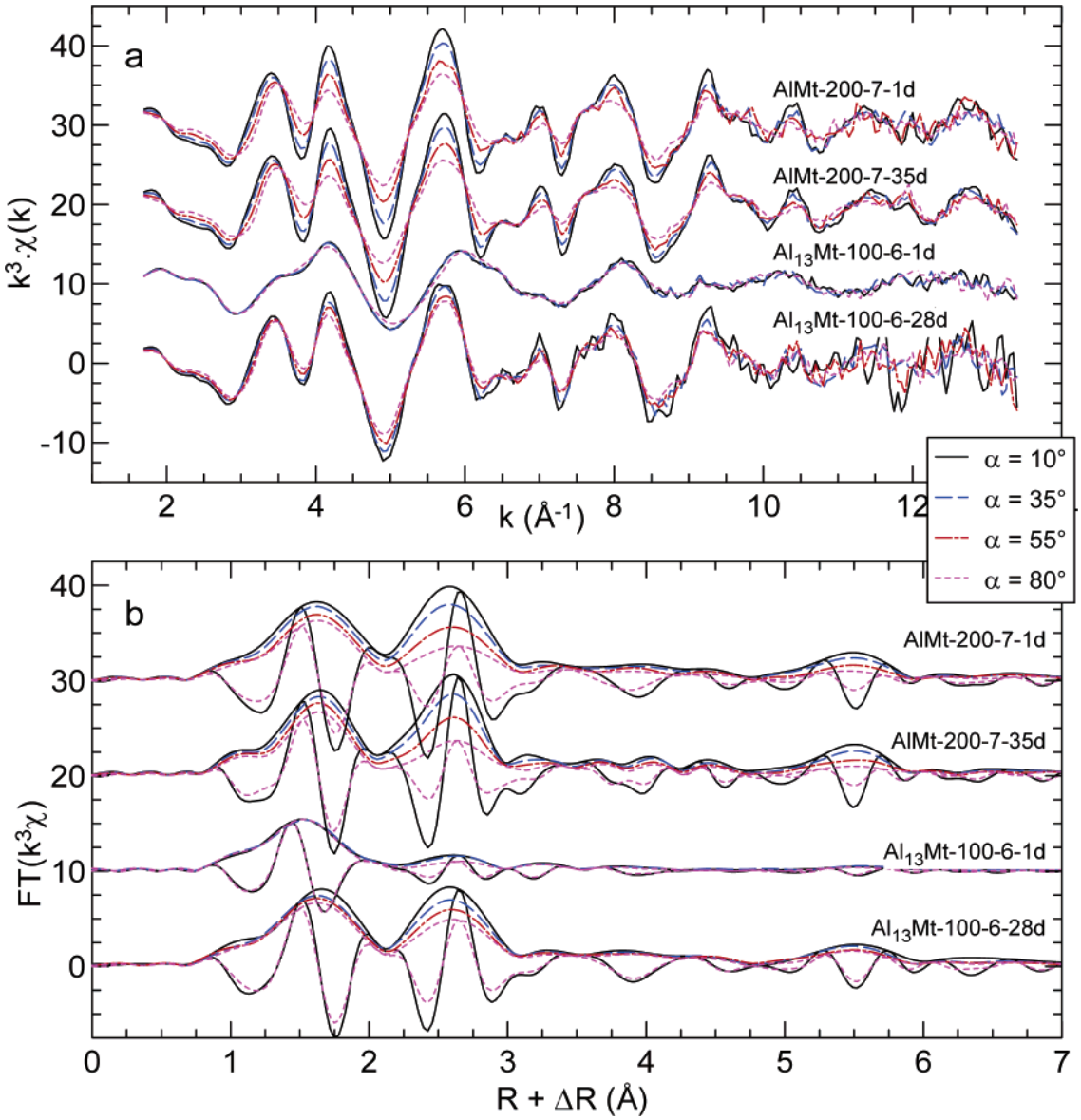

FIGURE 3. (a) k^3-weighted Zn K-edge P-EXAFS spectra and (b) moduli of the Fourier transforms (|FT|s) for Zn-sorbed Al-mont and Al_{13}-mont at α angles of 10°, 35°, 55°, and 80°. The imaginary part of the FTs at α = 10° and 80° are also plotted.

have been more complex, with peak extinction and shift in peak position at particular angles (*8*, *10*, *14*). Thus, P-EXAFS data indicate that the Al shell is oriented in plane, and that Zn has no nearest cationic shell in the out-of-plane direction.

Fair fits to all data with R_p values of about 0.08 were obtained with a single Al shell at $R_{Zn-Al}^{EXAFS} \approx 3.02-3.06(2)$ Å. This distance is characteristic of an edge linkage between Zn and Al octahedra. However, the number of Al neighbors for Al-mont samples and Al_{13}-Mt-100-6-28d derived from this fit ($N_{Al} \approx 8$ at α = 35°) significantly exceeded the maximum structural value of 6, which is attained when Zn occupies the vacant site of an $Al(OH)_3$ layer. In gibbsite, Al is surrounded by three pairs of second-nearest O atoms (O_2) at 3.19, 3.36, and 3.44 Å. The O_2 shell overlaps with the nearby Al shell and, thus, is hidden in the FT by the predominant Al contribution. Inclusion of the O_2 shell to the simulations, with $N_{Al} = N_{O2}$ to decrease the degree of freedom of the fit, decreased the figures of merit to $R_p \leq 0.034$ (Table S1), and provided optimal fits to the data with N_{Al} values close to 6 ($\sigma = 0.07-0.09$ Å) at α = 35° for all Al-mont samples and Al_{13}-Mt-100-6-28d. Since the O_2 contribution is minor, the Zn−Al distance was unchanged in the two-shell model, in agreement with previous studies (*9*, *23*, *31*). The average Zn−Al distance ($3.02(2) \leq R_{Zn-Al}^{EXAFS} \leq 3.06(2)$ Å) is 0.07−0.017 Å longer than the Al−Al distances in gibbsite (2.89−2.95 Å). Still, this increase is smaller than that predicted from the difference of ionic radii ($r^{VI}Zn^{2+} = 0.74$ Å; $^{VI}Al^{3+} = 0.53$ Å). The relaxation of the Zn site can be explained by a diminution of the electrostatic repulsion between Al^{3+} and Zn^{2+} in comparison to $Al^{3+}-Al^{3+}$ pairs. The Zn−Al + Zn−O_2 two-shell model also reproduced the decrease in amplitude of peak B with increasing α angle (Figure S3 in Supporting Information). Both N_{Al} and N_{O2} decreased with increasing α (Table S1), meaning that the Zn−Al and Zn−O_2 pairs have β angles with the normal to the film plane of >54.7°. This result confirms that the Zn-containing gibbsite-like layers are parallel to the montmorillonite layers (Figure 4a). The average $\beta_{Al,O2}$ angle, calculated from the angular dependence of N_{Al} and N_{O2} (*10*), is 67.3(8)° for AlMt-200-7-1d and 69(3)° for AlMt-200-7-35d. Similar values were reported for Ni in a gibbsite-like interlayer (*13*).

Peak C is located at about twice the distance of peak B, and results from the contribution of atoms at ~ 6 Å. In layer oxides and silicates, this peak arises from the third cationic shell (Me_3), and is amplified by Me−Me_1−Me_3 multiple scattering paths of the photoelectron (*32*) (Figure 4b). The

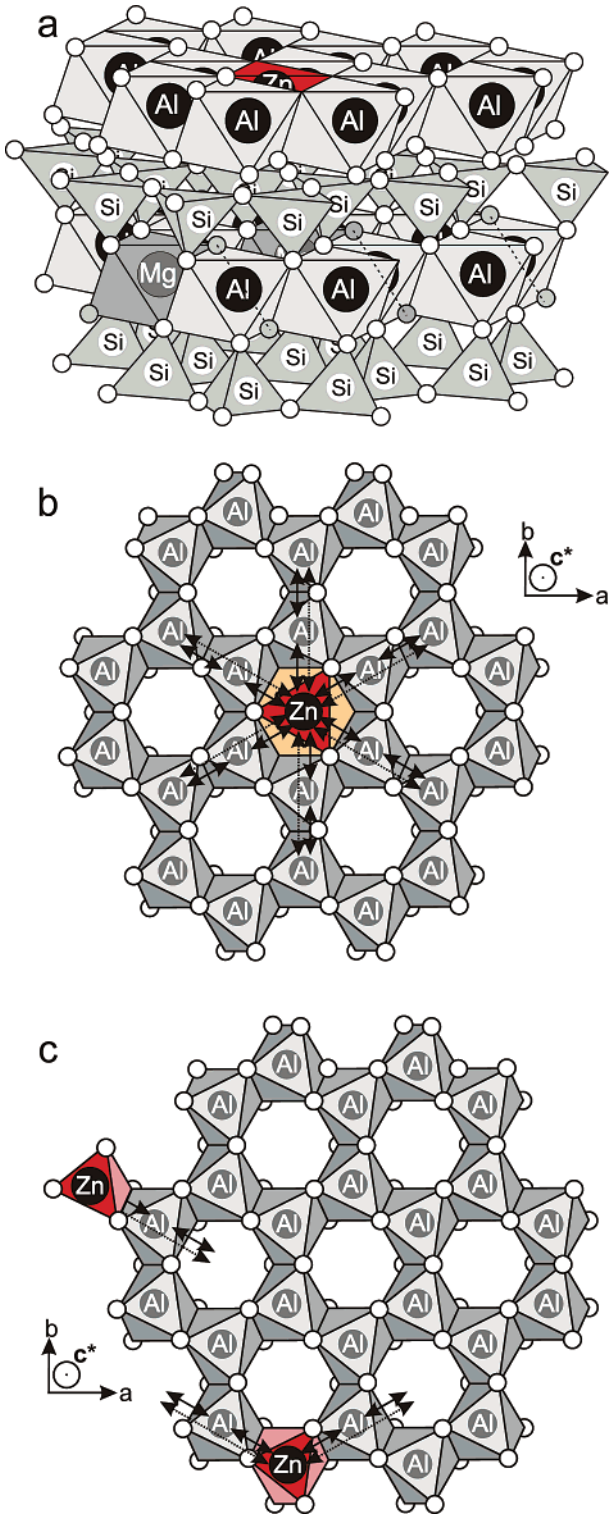

FIGURE 4. Structural models for Zn sorption on Al-mont and gibbsite (α-Al(OH)$_3$). (a) Zn-containing gibbsite layer on the basal plane of a montmorillonite layer. (b) Top view of a Zn-containing gibbsite layer. Arrows visualize the three and four leg (Zn−Al−Al) multiple scattering paths with an effective radius of ∼6 Å. (c) Zn sorption on the edges of a gibbsite layer. Note the absence of Al second-nearest neighbors at ∼6 Å (empty octahedra).

amplitude of the multiple scattering signal is sensitive to the collinearity of the three atoms (here Zn−Al−Al), and decreases rapidly with increasing deviation from 180° (*22*). Calculations performed on birnessite (MnO_2) layers showed that the signal is reduced by 50% for a dihedral angle of 170° and is completely attenuated for an angle of 160° (*33*). Thus, the prominence of peak C in Al-mont and Al_{13}-mont after 28 days of reaction is evidence of Zn in the middle of the gibbsite-like layer. Peak C is about five times weaker in Al_{13}Mt-100-6-1d than in Al-mont samples (Figure S4 in Supporting Information), and is absent in Zn-sorbed gibbsite.

Discussion

Mechanism of Zn Sorption on Gibbsite. The formation of mononuclear bidentate (i.e., edge-sharing) Zn complexes at the edges of gibbsite particles (Zn_{edge} complex) as proposed by Roberts et al. (*28*, *34*) is confirmed in the present study. This interpretation relied on the Zn−Al interatomic distance of $R \approx 3.0-3.1$ Å, and is now corroborated by the lack of Zn−Al−Al multiple scattering path, which manifests itself in the absence of peak C in the FT (Figure 2b and Figure S2 in Supporting Information). This result is strong evidence that Zn did not migrate into the vacant octahedral sites of gibbsite (Figure 4b), but sorbed on lateral sites (Figure 4c).

Mechanism of Zn sorption on Al-mont. Insight into the uptake mechanism of Zn on Al-mont is obtained from the comparison of AlMt-50-6-1d and Zn-sorbed-gibbsite data. Although the two samples were prepared at similar pH and reaction time, in AlMt-50-6-1d Zn is located in vacant octahedra of gibbsite-like layers ($^{VI}Zn_{layer}$). Diffusion into preexisting layer sites is unlikely, because this process did not occur in gibbsite. Thus, Zn probably coprecipitated with interlayer Al^{3+} cations to form Zn-containing hydroxy-Al layers. The resulting excess of positive charge in the dioctahedral Al layer can be balanced in several ways. The neutrality of the layer may be maintained by substituting three Zn^{2+} for two Al^{3+}. This charge compensation mechanism implies the presence of octahedral vacancies adjacent to a Zn site, which is inconsistent with $N_{Al} \approx 6$. Another possibility is the loss of two structural protons per Zn incorporated. The coexistence of protonated and unprotonated oxygens in oxyhydroxides causes dispersion of the cation−oxygen and cation−cation distances (*35*). Thus, this model is inconsistent with the low values of the EXAFS disorder parameter for the Zn−O and Zn−Al pairs ($\sigma = 0.08-0.09$ Å). The positive layer charge is balanced more likely by negative charges from sorbed anions or from interlayered smectite layers. The last possibility is more realistic for three reasons. First, only charge-balancing from interlayered smectite can explain the angular dependence of the EXAFS signal. Second, in lithiophorite, $Al(OH)_3$ layers that are positively charged by Li^+, Zn^{2+}, Ni^{2+}, or Cu^{2+} impurities at vacant octahedral sites are sandwiched between negatively charged MnO_2 layers (*18*, *36*). Third, the incorporation of Zn in the gibbsitic layer from hydroxy-Al mixed-layer phyllosilicate is common in acidic to near-neutral soils (*16*−*18*), and occurs at pHs (here at pH 6) for which little Zn is sorbed on phyllosilicate layers (*5*).

Zn incorporation in gibbsitic layers in contact with Al-mont was demonstrated previously by powder EXAFS (*37*). In this other study, $N_{Al} = 9.1$, a value much too high to be compatible with a layer structure, as in this case Zn does not have nearest Al neighbors in the out-of-plane direction. A likely reason for the overestimation of N_{Al} is the omission of the O_2 shell in the previous data analysis.

Mechanism of Zn Sorption on Al_{13}-mont. After 1 day of contact time at pH 6, Zn is dominantly tetrahedral and secondarily octahedral at the Al_{13}-mont surface, whereas it is uniquely octahedral in solution (*38*). The small number of nearest Al neighbors ($N_{Al} \approx 1$), oriented in the film plane, suggests the formation of Zn_{edge} surface complexes, whereas the existence of Zn−Al−Al multiple scattering paths is an indication of Zn_{layer} complexes. The possible coexistence of Zn_{edge} and Zn_{layer} species when aluminum is added in polymeric instead of monomeric form can be explained by the low amount of free Al^{3+} cations that can coprecipitate with Zn. Based on the amplitude of peak C, the proportion

of Zn_{layer} to total Zn is ≤20%, and so the weighted number of nearest Al neighbors for this Zn species is $N_{Al} = 0.2 \times 6 = 1.2$. This number is identical to the experimental value (1.0(5), Table S1). Thus, no nearest Al neighbors seem to be detected for Zn_{edge}, due possibly to structural disorder caused by the coexistence of $^{IV}Zn_{edge}$ and $^{VI}Zn_{edge}$ surface species.

After 28 days, Zn has the same binding environment as in Al-mont. Zn incorporation in gibbsite-like layers with time is possible if more Al becomes available for coprecipitation. At near-neutral pH, Al_{13} polymers are generally unstable, and progressively transform to amorphous $Al(OH)_3$(s) or bayerite ($Al(OH)_3$) in a few days (*27*). Some of the dissolved Al may have coprecipitated with Zn, leading to the formation of Zn-containing gibbsitic layers. In this case, Zn incorporation is controlled by the supply of dissolved Al, i.e., the destabilization of Al_{13} polymers: the longer the reaction time, the higher the amount of dissolved Al, and the greater the proportion of Zn in gibbsite-like sheets. However, some Al may also have formed weakly charged colloids, competing with gibbsitic interlayers for Zn uptake. A Zn association with $Al(OH)_3$ colloids would explain why 67% of total Zn remained in the supernatant after 28 days of reaction (Figure 1a).

Implication for Zinc Sequestration. Independent of the degree of polymerization of Al in the montmorillonite interlayer, Zn ended up in the vacant octahedral sites of gibbsite-like layers at the basal and/or interlayer surfaces of montmorillonite particles. This incorporation mechanism can lead to long-term sequestration of Zn, as shown experimentally (*37*) and by the presence of Zn-containing hydroxy-Al phyllosilicate in natural soils (*16*−*18*). Gibbsitic layers can be intercalated also between MnO_2 layers by Al^{3+} or Al_{13} exchange to form lithiophorite (*39*, *40*) and, consequently, Zn may be incorporated also in this mixed-layer Mn oxide (*18*, *41*). Therefore, amending contaminated soils with aluminum is a possible remediation strategy, especially in slightly acidic soils in which Zn immobilization by precipitation of pure or mixed hydroxides, or sorption on iron oxyhydroxides, may fail.

The empty sites of gibbsite layers may be filled with cations other than Zn, but of comparable size. This is the case for Li (*36*), Ni (*13*, *42*), and Cu (*43*), whose cation−hydroxyl distances (d^{VI}(Li−OH) ≈ 2.10 Å; d^{VI}(Ni−OH) ≈ 2.03 Å; d^{VI}(Cu−OH) ≈ 1.9−2.2 Å) are commensurate with the distance separation between OH groups and the center of a vacant octahedron (2.11 Å). Heavy rare earth elements (e.g., d^{VI}(Lu−OH) ≈ 2.20 Å) may also enter this site, provided the excess of charge due to the incorporation of a trivalent cation in the Al layer can be balanced. In contrast, trivalent actinides and light rare earth elements may be too big (e.g., d^{VI}(Am−OH) ≈ 2.31 Å; d^{VI}(La−OH) ≈ 2.37 Å; (*44*)) to enter this site.

Acknowledgments

Several reference EXAFS spectra used in this study were provided by A.C. Scheinost and D.R. Roberts. J.L. Hazemann and O. Proux are thanked for their assistance during EXAFS measurements on FAME at ESRF. This work was supported by the French-CRG program from CNRS and by DEN/DDIN/HAVL from CEA.

Note Added After ASAP Publication

There were some errors in Figure 3 in the version published ASAP February 17, 2007; the corrected version was published ASAP February 22, 2007.

Supporting Information Available

Figure S1, concentrations of dissolved Si and Al for sorption experiments; Figure S2, FTs from powder EXAFS data for Zn sorption samples and Zn-containing structural references; Figure S3, spectral simulations of the FTs from P-EXAFS data; Figure S4, FT amplitudes and imaginary parts of peaks B and C for Al_{13}Mt-100-6-1d and Al_{13}Mt-100-6-28d; Table S1, structural parameters from the modeling of EXAFS data. This material is available free of charge via the Internet at http://pubs.acs.org.

Literature Cited

(1) Brookins, D. G. *Geochemical Aspects of Radioactive Waste Disposal*; Springer-Verlag: Berlin, 1984.
(2) Saha, U. K.; Taniguchi, S.; Sakurai, K. Simultaneous adsorption of cadmium, zinc, and lead on hydroxyaluminum- and hydroxyaluminosilicate-montmorillonite complexes. *Soil Sci. Soc. Am. J.* **2002**, *66*, 117−128.
(3) Harsh, J. B.; Doner, H. E. Specific adsorption of copper on an hydroxy-aluminum complex. *Soil Sci. Soc. Am. J.* **1984**, *48*, 1034−1038.
(4) Furrer, G.; Zysset, M.; Schindler, P. W. Weathering kinetics of montmorillonite: investigations in batch and mixed-flow reactors. In *Geochemistry of Clay-Pore-Fluids Interactions*; Manning, D. A. C., Hall, P. L., Hughes, C. R., Eds.; Chapman & Hall: London, 1993; pp 243−262.
(5) Lothenbach, B.; Furrer, G.; Schulin, R. Immobilization of heavy metals by polynuclear aluminium and montmorillonite compounds. *Environ. Sci. Technol.* **1997**, *31*, 1452−1462.
(6) Lothenbach, B.; Furrer, G.; Schärli, H.; Schulin, R. Immobilization of zinc and cadmium by montmorillonite compounds: effects of aging and subsequent acidification. *Environ. Sci. Technol.* **1999**, *33*, 2945−2952.
(7) Manceau, A.; Chateigner, D.; Gates, W. P. Polarized EXAFS, distance-valence least-squares modeling (DVLS) and quantitative texture analysis approaches to the structural refinement of Garfield nontronite. *Phys. Chem. Miner.* **1998**, *25*, 347−365.
(8) Schlegel, M. L.; Manceau, A.; Chateigner, D.; Charlet, L. Sorption of metal ions on clay minerals. I. Polarized EXAFS evidence for the adsorption of cobalt on the edges of hectorite particles. *J. Colloid Interface Sci.* **1999**, *215*, 140−158.
(9) Schlegel, M. L.; Manceau, A.; Hazemann, J.-L.; Charlet, L. Adsorption mechanisms of Zn on hectorite as a function of time, pH, and ionic strength. *Am. J. Sci.* **2001**, *301*, 798−830.
(10) Schlegel, M. L.; Manceau, A.; Charlet, L.; Chateigner, D.; Hazemann, J.-L. Sorption of metal ions on clay minerals. III. Nucleation and epitaxial growth of Zn phyllosilicate on the edges of hectorite. *Geochim. Cosmochim. Acta* **2001**, *65*, 4155−4170.
(11) Dähn, R.; Scheidegger, A. M.; Manceau, A.; Schlegel, M. L.; Baeyens, B.; Bradbury, M. H.; Morales, M. Neoformation of Ni phyllosilicate upon Ni uptake by montmorillonite. A kinetics study by powder and polarized extended X-ray absorption fine structure spectroscopy. *Geochim. Cosmochim. Acta* **2002**, *66*, 2335−2347.
(12) Dähn, R.; Scheidegger, A. M.; Manceau, A.; Schlegel, M. L.; Baeyens, B.; Bradbury, M. H.; Morales, M. Structural evidence for the sorption of metal ions on the edges of montmorillonite layers. A polarized EXAFS study. *Geochim. Cosmochim. Acta* **2003**, *67*, 1−15.
(13) Nachtegaal, M.; Scheidegger, A. M.; Dähn, R.; Chateigner, D.; Furrer, G. Immobilization of Ni by Al-modified montmorillonite: A novel uptake mechanism. *Geochim. Cosmochim. Acta* **2005**, *69*, 4211−4225.
(14) Schlegel, M. L.; Manceau, A. Evidence for the nucleation and epitaxial growth of Zn phyllosilicate on montmorillonite. *Geochim. Cosmochim. Acta* **2006**, *70*, 901−917.
(15) Furnare, L. J.; Vailionis, A.; Strawn, D. G. Polarized XANES and EXAFS spectroscopic investigation into copper(II) complexes on vermiculite. *Geochim. Cosmochim. Acta* **2005**, *69*, 5219−5231.
(16) Scheinost, A. C.; Kretzschmar, R.; Pfister, S. Combining selective sequential extractions, x-ray absorption spectroscopy, and principal component analysis for quantitative zinc speciation in soil. *Environ. Sci. Technol.* **2002**, *36*, 5021−5028.
(17) Manceau, A.; Marcus, M. A.; Tamura, N.; Proux, O.; Geoffroy, N.; Lanson, B. Natural speciation of Zn at the micrometer scale in a clayey soil using X-ray fluorescence, absorption, and diffraction. *Geochim. Cosmochim. Acta* **2004**, *68*, 2467−2483.
(18) Manceau, A.; Tommaseo, C.; Rihs, S.; Geoffroy, N.; Chateigner, D.; Schlegel, M.; Tisserand, D.; Marcus, M. A.; Tamura, N.; Chen, Z.-S. Natural speciation of Mn, Ni and Zn at the micrometer scale in a clayey paddy soil using X-ray fluorescence, absorption, and diffraction. *Geochim. Cosmochim. Acta* **2005**, *69*, 4007−4034.

(19) Tournassat, C.; Neaman, A.; Villieras, F.; Bosbach, D.; Charlet, L. Nanomorphology of montmorillonite particles: Estimation of the clay edge sorption site density by low-pressure gas adsorption and AFM observations. *Am. Miner.* **2003**, *88*, 1989−1995.
(20) Tournassat, C.; Greneche, J. M.; Tisserand, D.; Charlet, L. The titration of clay minerals I. Discontinuous backtitration technique combined with CEC measurements. *J. Colloid Interface Sci.* **2004**, *273*, 224−233.
(21) Proux, O.; Nassif, V.; Prat, A.; Ulrich, O.; Lahera, E.; Biquard, X.; Menthonnex, J.-J.; Hazemann, J.-L. Feedback system of a liquid-nitrogen-cooled double-crystal monochromator: design and performances. *J. Synchrotron Radiat.* **2006**, *13*, 59−68.
(22) Teo, B. K. *EXAFS: Basic Principles and Data Analysis*; Springer-Verlag: Berlin, 1986.
(23) Manceau, A.; Combes, J.-M. Structure of Mn and Fe oxides and oxyhydroxides: a topological approach by EXAFS. *Phys. Chem. Miner.* **1988**, *15*, 283−295.
(24) Michot, L. J.; Barres, O.; Hegg, E. L.; Pinnavaia, T. J. Cointercalation of Al_{13} polycations and nonionic surfactants in montmorillonite clay. *Langmuir* **1993**, *9*, 1794−1800.
(25) Nagy, K. L. Dissolution and precipitation kinetics of sheet silicates. In *Chemical Weathering Rates of Silicate Minerals*; White, A. F., Brantley, S. L., Eds.; Mineralogical Society of America: Washington, DC, 1995; Vol. 31, pp 173−233.
(26) Stumm, W.; Morgan, J. J. *Aquatic Chemistry*, 3rd ed.; John Wiley & Sons: New York, 1996.
(27) Bottero, J. Y.; Axelos, M.; Tchoubar, D.; Cases, J. M.; Fripiat, J. J.; Fiessinger, F. Mechanism of formation of aluminum trihydroxide from keggin Al_{13} polymers. *J. Colloid Interface Sci.* **1987**, *117*, 47−57.
(28) Roberts, D. R.; Ford, R. G.; Sparks, D. L. Kinetics and mechanisms of Zn complexation on metal oxides using EXAFS spectroscopy. *J. Colloid Interface Sci.* **2003**, *263*, 364−376.
(29) Manceau, A.; Schlegel, M. L.; Musso, M.; Sole, V. A.; Gauthier, C.; Petit, P. E.; Trolard, F. Crystal chemistry of trace elements in natural and synthetic goethite. *Geochim. Cosmochim. Acta* **2000**, *64*, 3643−3661.
(30) Sarret, G.; Manceau, A.; Spadini, L.; Roux, J. C.; Hazemann, J.-L.; Soldo, Y.; Eybert-Berard, L.; Menthonnex, J.-J. Structural determination of Zn and Pb binding sites in *Penicillium chrysogenum* cell walls by EXAFS spectroscopy. *Environ. Sci. Technol.* **1998**, *32*, 1648−1655.
(31) Villalobos, M.; Lanson, B.; Manceau, A.; Toner, B.; Sposito, G. Structural model for the biogenic Mn oxide produced by *Pseudomonas putida*. *Am. Miner.* **2006**, *91*, 489−502.
(32) O'Day, P. A.; Rehr, J. J.; Zabinsky, S. I.; Brown, G. E., Jr. Extended X-ray absorption fine structure (EXAFS) analysis of disorder and multiple-scattering in complex crystalline solids. *J. Am. Chem. Soc.* **1994**, *116*, 2938−2949.
(33) Ressler, T.; Brock, S. L.; Wong, J.; Suib, S. L. Multiple-scattering EXAFS analysis of tetraalkylammonium manganese oxide colloids. *J. Phys. Chem. B* **1999**, *103*, 6407−6420.
(34) Roberts, D. R.; Scheinost, A. C.; Sparks, D. L. Zinc speciation in a smelter-contaminated soil profile using bulk and microspectroscopic techniques. *Environ. Sci. Technol.* **2002**, *36*, 1742−1750.
(35) Szytula, A.; Burwicz, A.; Dimitrijevic, Z.; Kraznicki, S.; Rzany, H.; Todorovic, J.; Wanic, A.; Wolski, W. Neutron diffraction studies of α-FeOOH. *Phys. Status Solidi* **1968**, *26*, 429−434.
(36) Post, J. E.; Appleman, D. E. Crystal structure refinement of lithiophorite. *Am. Miner.* **1994**, *79*, 370−374.
(37) Nachtegaal, M.; Scheidegger, A. M.; Dahn, R.; Chateigner, D.; Furrer, G. The role of Al in Zn Immobilization by montmorillonite. *Trans. Utrecht Univ. Geol. Survey* **2006**, *7*, 27−34.
(38) Waychunas, G. A.; Fuller, C. C.; Davis, J. A. Surface complexation and precipitate geometry for aqueous Zn(II) sorption on ferrihydrite: I. X-ray absorption extended fine structure analysis. *Geochim. Cosmochim. Acta* **2002**, *66*, 1119−1137.
(39) Feng, Q.; Horiuchi, T.; Liu, L. H.; Yanagisawa, K.; Mitsushio, T. Hydrothermal soft chemical reaction for formation of sandwich layered manganese oxide. *Chem. Mater.* **1999**, *11*, 2444−2450.
(40) Yang, D. S.; Wang, M. K. Characterization and a fast method for synthesis of sub-micron lithiophorite. *Clays Clay Miner.* **2003**, *51*, 96−101.
(41) Manceau, A.; Tamura, N.; Celestre, R. S.; MacDowell, A. A.; Geoffroy, N.; Sposito, G.; Padmore, H. A. Molecular-scale speciation of Zn and Ni in soil ferromanganese nodules from loess soils of the Mississippi Basin. *Environ. Sci. Technol.* **2003**, *37*, 75−80.
(42) Manceau, A.; Llorca, S.; Calas, G. Crystal chemistry of cobalt and nickel in lithiophorite and asbolane from New Caledonia. *Geochim. Cosmochim. Acta* **1987**, *51*, 105−113.
(43) Manceau, A.; Buseck, P. R.; Miser, D.; Rask, J.; Nahon, D. Characterization of Cu from a banded Mn ore. *Am. Mineral.* **1990**, *75*, 490−494.
(44) Shannon, R. D. Revised effective ionic radii and systematic studies of interatomic distances in halides and chalcogenides. *Acta Crystallogr.* **1976**, *A32*, 751−767.

Received for review August 14, 2006. Revised manuscript received December 21, 2006. Accepted January 8, 2007.

ES061958I